Ain Shams Engineering Journal (2012) 3, 33–48

Ain Shams University

Ain Shams Engineering Journal

www.elsevier.com/locate/asej
www.sciencedirect.com

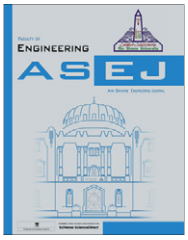

MECHANICAL ENGINEERING

An experimental study of freezing and melting of water inside spherical capsules used in thermal energy storage systems

Reda I. ElGhnam *, Ramdan A. Abdelaziz, Mohamed H. Sakr, Hany E. Abdelrhman

Faculty of Engineering, Benha University, Egypt

Received 31 May 2011; accepted 23 October 2011
Available online 26 December 2011

KEYWORDS

Freezing and melting;
Spherical capsules;
Thermal energy storage

Abstract This paper reports the results of an experimental study on the heat transfer during freezing (charging) and melting (discharging) of water inside a spherical capsule of the type often found in the beds of thermal (ice) storage systems used for the building air conditioning systems. Spherical capsules of different diameters and materials are tested. The aqueous solution of 35-wt% ethylene glycol is used as the heat transfer fluid (HTF). The major studied parameters are the size and material of the spherical capsule, the volume flow rate and temperature of the heat transfer fluid (HTF). The effects of these parameters on the time for complete charging/discharging, the solidified/melted

Abbreviations: Act, actual; CTES, cool thermal energy storage; ERR, energy recovery ratio; HTF, heat transfer fluid; PCM, phase change material; rot, rotameter; tc, thermocouple; TES, thermal energy storage

* Corresponding author. Tel.: +20 111150706; fax: +20 242158823.
E-mail addresses: reda_i_elghnam@yahoo.com (R.I. ElGhnam), ramadanamer2004@yahoo.com (R.A. Abdelaziz), mohamed.sakr@feng.bu.edu.eg (M.H. Sakr), hany_assawy2003@yahoo.com (H.E. Abdelrhman).

Peer review under responsibility of Ain Shams University.
doi:10.1016/j.asej.2011.10.004

Production and hosting by Elsevier

mass fraction, the charging/discharging rate, the energy stored/regain, and the energy recovery ratio (ERR) are studied. The experimental results show that the energy recovery ratio is becoming better when using metallic capsules, increasing the capsule size and reducing the HTF volume flow rates.

Nomenclature

C_i	specific heat of ice, kJ/kg K
C_w	specific heat of water, kJ/kg K
d_{in}	inside diameter of test capsule, m
F_O	Fourier number, $F_O = \alpha_i \times t/r_{in}^2$
k_i	thermal conductivity of ice, kW/m K
$L.H.$	latent heat of fusion of water, kJ/kg
m_m	melted mass, kg
m_o	mass of PCM encapsulated inside the spherical capsule, kg
m_s	solidified mass, kg
m_m/m_o	melted mass fraction
m_s/m_o	solidified mass fraction
$\dot{Q}_{ch}$	charging rate, kW
$\dot{Q}_{dis}$	discharging rate, kW
Q_{reg}	accumulative energy regained, kJ
Q_{st}	accumulative energy stored, kJ
$Q_{st,max}$	maximum energy stored at the complete charging time, kJ
$Q_{reg,max}$	maximum energy regained at the complete charging time, kJ
$r_{avg_{h,v}}$	average radius of solid–liquid interface in test capsule, m
r_h	horizontal radius of solid–liquid interface in test capsule, m
r_{in}	inside radius of test capsule, m
r_v	vertical radius of solid–liquid interface in test capsule, m
T_{act}	actual temperature, °C
T_c	temperature of PCM at the center of capsule, °C
T_l	liquid phase temperature of PCM, °C
T_o	initial temperature of PCM (distilled water), °C
T_{pc}	phase change temperature, °C
T_s	solid phase temperature of PCM, °C
T_{tc}	thermocouple temperature reading, °C
T^*	dimensionless temperature, $T^* = T_c/T_{pc}$
t	time, s
$t_{comp.ch}$	complete charging time, s
$t_{comp.dis}$	complete discharging time, s
Δt	time difference, s
V_m	Melted volume, m^3
V_s	solidified volume, m^3
V_{shell}	spherical shell volume, m^3
$\dot{V}_{act}$	actual volume flow rate, Lpm
$\dot{V}_{rot}$	volume flow rate obtained from the rotameter reading, Lpm
V_o	volume of the PCM encapsulated inside the spherical capsule (equal to 80% of internal volume of the capsule), m^3

Greek symbols

ρ_w	water density, kg/m^3
ρ_i	ice density, kg/m^3
ρ_w/ρ_i	volume correction factor
α_i	thermal diffusivity of ice $(= k_i/\rho_i C_i)$, m^2/s
τ	dimensionless time, $(\tau = F_o = \alpha_i \times /r_{in}^2)$
$\tau_{comp.ch}$	dimensionless complete charging time
$\tau_{comp.dis}$	dimensionless complete discharging time
α_i	thermal diffusivity of ice
ΔQ_{reg}	accumulative thermal energy regained difference, kJ
ΔQ_{st}	accumulative thermal energy stored difference, kJ
Δt	time difference, s

1. Introduction

Studying the thermal behavior during phase change in spherical capsules is extremely important for the design of efficient storage systems. Some experimental and theoretical studies investigations concerning the cool thermal energy storage (CTES) of encapsulated type are found in literature.

Eames and Adref [1] conducted an experimental study of the freezing and melting processes for water contained in spherical elements. They reported quantitative data on the movement of the solid–liquid interface position with time, the effect of HTF (coolant) temperature, and the effect of sphere size on the melting and freezing processes. They also reported the discharge and charge rates and the time required to melt and freeze a spherical ice storage element. Finally, their results were used to derive empirical equations describing charge and discharge for an ice storage element.

Yoon et al. [2] studied experimentally the freezing phenomenon of saturated water with the supercooled region in a horizontal circular cylinder. From the experiments, it was found that there were three types of freezing patterns. The first was the annular ice layer growing from the cylinder surface at a high cooling rate, the second was the asymmetric ice layer at an intermediate cooling rate, and the last was the instantaneous ice layer growing over the whole region at a low cooling rate.

Ismail et al. [3] presented the results of a numerical study on the heat transfer during the process of solidification of water inside a spherical capsule under convective boundary conditions. The numerical solution was based upon the finite

difference approach and the moving grid scheme. They also validated the numerical predictions by comparison with experimental results realized by the authors. The size of the spherical capsule, wall material, external bath temperature and initial temperature of water were investigated and their effects on the solidified mass fraction and the time for complete solidification were presented and discussed.

Sakr et al. [4] conducted experimental and theoretical study on freezing and melting in capsules with different configurations. They used water as a phase change material (PCM). The PCM was encapsulated in five different copper capsules (sphere, cylinder, pyramid, cone, and cuboids) having the same internal volume. The effect of geometrical configuration on the characterization of the freezing and melting processes was investigated. The spherical capsule showed the best thermal energy storage performance among the five test configurations.

Tan et al. [5] reported an experimental and computational investigation directed at understanding the role of buoyancy-driven convection during constrained melting of phase change material (PCM) inside a spherical capsule. The melting phase front and melting fraction of the PCM were analyzed and compared with numerical solution obtained from the CFD code Fluent. They observed expedited phase change in the top region of the sphere and a wavy surface at the bottom of the PCM after a short period of symmetric melting due to prominence of diffusion.

Cheralathan et al. [6] investigated the transient behavior of phase change material based cool thermal energy storage (CTES). The system discussed was comprised of a cylindrical storage tank filled with encapsulated phase change materials (PCMs) in spherical container integrated with an ethylene glycol chiller plant. A simulation program was developed to evaluate the temperature history of the heat transfer fluid (HTF) and the phase change material at any axial location during the charging period. The model was also used to investigate the effect of porosity, Stanton number, Stefan number and Peclet number on CTES system performance. The results showed that increase in porosity contributes to a higher rate of energy storage. However, for a given geometry and heat transfer coefficient, the mass of PCM charged in the unit was found to decrease as the increase in porosity.

Kousksou et al. [7] investigated numerically the influences of the position of the storage tank and the flow pattern inside the tank for a cylindrical tank randomly filled with PCM encapsulated in spherical capsules. They used two-dimensional porous-medium modeling in two configurations of storage: vertical configuration where the stream lines of natural convection are in the same direction as the forced convection and the horizontal configuration where the natural convection is preponderant on that forced convection They reported that the optimum running of the charge mode is obtained in the case of a vertical position where the motions due to the natural convection are in the same direction as the forced convection.

Ismail and Henriquez [8] presented a numerical study of the solidification of PCM (distilled water) enclosed in a spherical shell. The mathematical model was based on pure conduction in the PCM subject to boundary conditions of constant temperature or convection heat transfer on the external surface of the spherical shell. The model was then used to predict the effect of the size of the spherical shell, shell thickness, shell material, initial PCM temperature and the external wall temperature on the solidified mass fraction and the time for complete solidification.

Kalaiselvam et al. [9] conducted analytical solutions for solidification and melting process of different PCMs encapsulated inside cylindrical enclosures. Their study aimed to find the interface locations at various time steps. Transient interface positions and complete phase change time were predicted by two models for solidification and by three models for melting. Their analytical model was used to study the phase change behavior and heat transfer characteristics inside PCM. Presence of heat generation increased the total solidification time of the cylinder, though it accelerated melting. Total solidification time depended on Stefan Number and heat generation parameter, whereas complete melting time depended on equivalent thermal conductivity.

Similar investigations were reported by many other authors, eg. Khodadadi, and Zhang [10], Wu et al. [11], MacPhee and Dincer [12], Erek and Dincer [13], MacPhee and Dincer [14], Ananthanarayanan et al. [15], Beasley and Ramanarayanan [16], Sozen et al. [17] and Ismail and Stuginsky [18].

2. Description of experimental test rig

The main target of the current study is to investigate experimentally the effect of the size and material of the spherical capsule (storage element), the volume flow rate and temperature of heat transfer fluid (HTF) on the time for complete charging/discharging, the solidified/melted mass fraction, the percentage of energy stored/regained, and the energy recovery ratio (ERR). To accomplish the above needs, a test rig is designed and manufactured to carry out the heat transfer experiments using the suitable instrumentation.

The test rig used in the present study is shown schematically in Fig. 1a. It consists of charging tank, discharging tank, spherical capsule (test section), refrigeration unit, heating section, heat transfer fluid circulation unit (centrifugal pump, piping system, gate valves), and suitable measuring instrumentation. The test rig components will be described in details through the following sections. The heat transfer fluid (HTF) is selected to be aqueous ethylene glycol solution which has a concentration of 35% by weight. The chosen concentration has a freezing point of -19 °C, [19].

2.1. Charging and discharging tanks

The charging and discharging tanks have the same dimensions. They are galvanized steel tanks having dimensions of $350 \times 350 \times 450$ mm, and painted internally by chemical coating (epoxy). To reduce the heat gain; the tanks are insulated by a 50 mm thickness of injected expanded polyurethane thermal insulation. Each tank is filled with a 0.038 m^3 of the HTF. The two tanks are provided with inlet and outlet pipes including manual gate valves for the HTF circulation. Also, they are provided with a movable insulated door at their tops.

2.2. Spherical capsule (test section)

In the present study the spherical capsules represent the thermal storage test elements which made from different materials (copper, brass, stainless steel, glass, and plastic) and having different internal diameters (0.042, 0.07, 0.092, 0.10, and 0.11) with the same thickness (0.001 m) are employed to carry

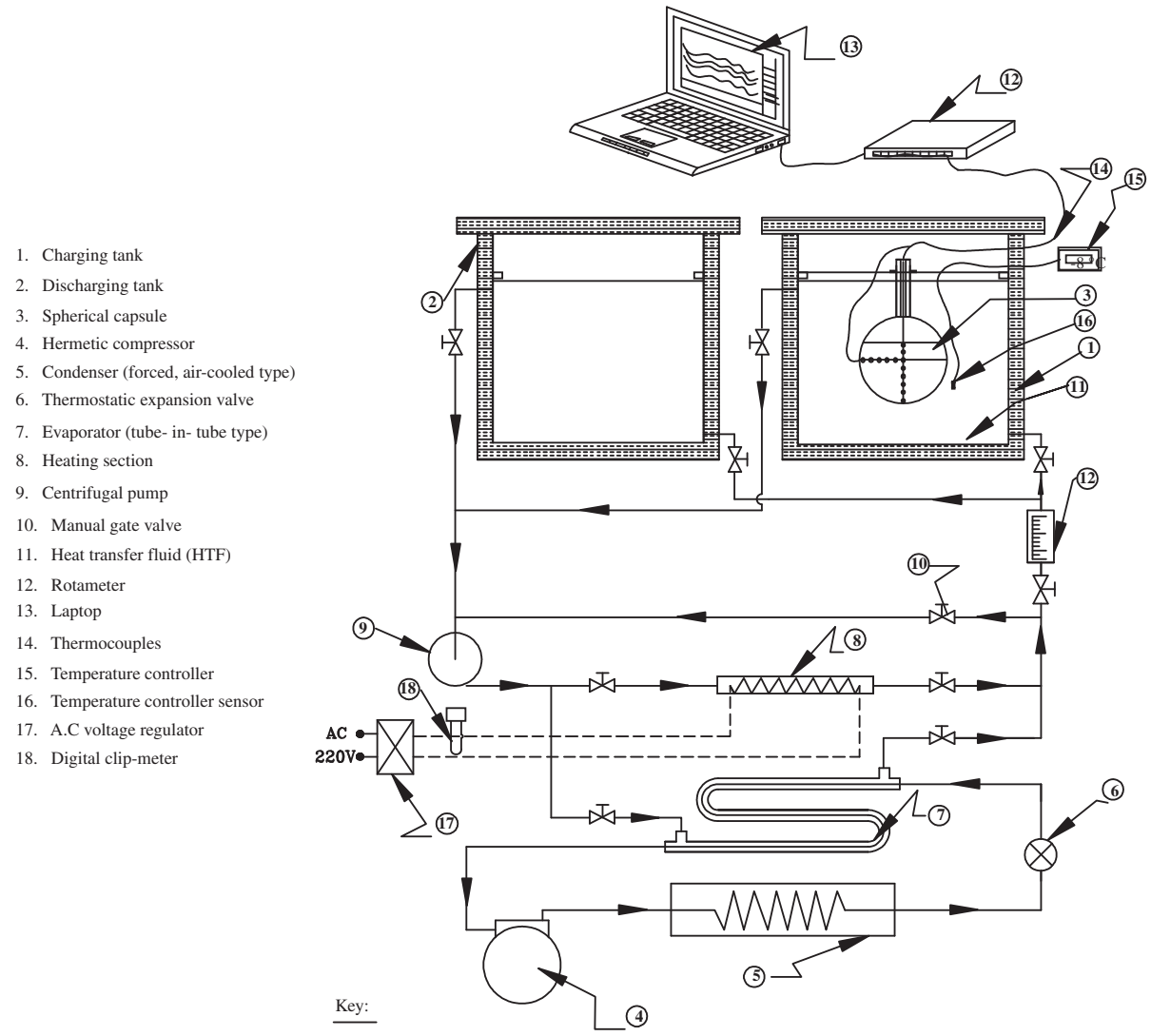

Figure 1a Line diagram of the test rig.

out the experiments. The capsule materials are selected to introduce a wide range of thermal conductivity. Distilled water is used as the phase change material (PCM). Each one of the spherical capsules is filled by 80% of its inner volume with distilled water as a PCM to avoid the thermal expansion during the solidification process. Fifteen calibrated copper-constantan (T-type) thermocouples are employed to measure the temperature distribution. Thirteen of them are distributed on the horizontal and vertical axes of the spherical capsule at specified distances, as shown in Fig. 1b, and the other two thermocouples are used to measure the HTF temperature around the spherical capsule.

2.3. Refrigeration unit and electric heating section

The refrigeration unit is a simple vapor-compression cycle, operated with R-22. It includes a hermetic compressor (3 hp), air cooled condenser (forced type), filter, drier, thermostatic expansion valve, and an evaporator (tube-in-tube type). The main purpose of the refrigeration unit is to cool the HTF to a specified temperature to achieve the requirements of the charging process.

The main purpose of the electric heating section is to heat the HTF to a specified temperature, to achieve the requirements of the discharging process. The heating section is a copper pipe with an outer diameter of 0.0218 m. It is externally wrapped with an electric resistance (200 W heating capacity), then electrically and thermally insulated. The electric resistance is connected to AC voltage regulator (0–220 V), to enable electric power control.

A digital temperature controller (electronic thermostat) is employed to control the required temperature inside the discharging tank and charging tank with a set-point differential of ± 1 °C.

2.4. HTF circulation unit and piping system

A centrifugal pump is used to circulate the HTF through the piping system to carry out the charging and discharging experiments. The piping system and the manual gate valves are

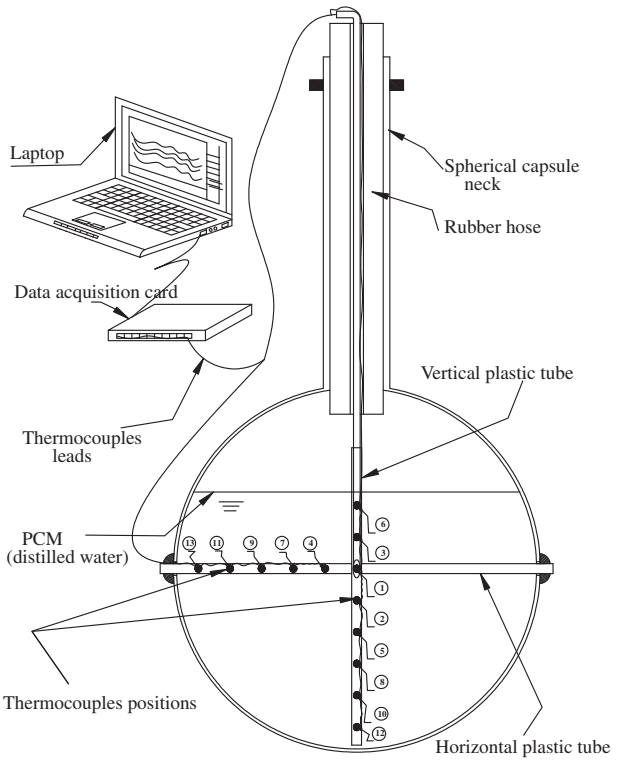

Figure 1b Test section details showing distribution of thermocouples.

Table 1 Experimental parameters.

HTF parameters	
Temperature (during charge process)	−4, −6, −8, −10, and −12 °C
Temperature (during discharge process)	6, 8, 10, 12, and 14 °C
Volume flow rate	1, 3, 4, 5, and 7 Lpm
Spherical capsule parameters	
Size (internal diameter)	0.042, 0.07, 0.092, 0.11, and 0.126 m
Material	Copper, brass, stainless steel, glass, and plastic

arranged to enable the same pump to circulate the heat transfer fluid through the charging and discharging cycles. The discharge pipe connected to the centrifugal pump is branched into two parallel lines; one of them to the heating section and the other to the evaporator of the refrigeration unit. The two branches are integrated with manual gate valves at inlet and outlet of the heating section and the evaporator. The common pipe line after the heating section and the evaporator is separated into two lines; one of them is directed to the rotameter and then to the charging or discharging tank and the other is bypassed to the suction line of the pump to achieve volume flow rate control.

2.5. Measuring instruments

Suitable measuring instruments are used for monitoring temperatures and HTF volume flow rates. A data acquisition card (National Instruments, NI USB-6210, 16-inputs, resolution of 16-bit and scanning rate of 250 kS/s) and a laptop are used to monitor the temperatures through fifteen calibrated copper-constantan (T-type) thermocouples. The HTF volume flow rate is monitored by using a calibrated rotameter. To control a certain flow rate as an experimental parameter; a manual gate valve and a bypass pipe fitted with another manual gate valve are installed before the rotameter. A digital temperature controller (electronic thermostat) is used to control the required temperature inside the charging or discharging tank during the charging and discharging experiments, respectively. The specifications of the digital temperature controller are (ELIWELL IC 901, 0.5% accuracy, and 1 °C set-point differential). A digital AC voltage regulator is used to adjust the input power to the heating section.

3. Experimental procedures

A series of charging and discharging experiments are performed under various parameters. The varied parameters in the present study are listed in Table 1. The charging and discharging experiments are conducted, respectively and their experimental procedures are discussed in the following two sections.

The manual gate valves incorporated with the piping system are positioned for the charging mode, and the refrigeration unit operates to cool the circulating HTF. The digital temperature controller is set at one of the five test temperatures mentioned in Table 1. The PCM temperature is maintained at 25 °C as an initial PCM temperature for all charging experiments. Once the adjusted HTF temperature reaches, the volume flow rate of the HTF is set at one of the five volume flow rates mentioned in Table 1. Measurements of the PCM temperatures inside the test capsule and the HTF temperatures around it are scanned and recorded every two seconds by the data acquisition system. The experiment is terminated when the temperature of the PCM inside the test capsule starts to be equal to that of the HTF. This indicates that the water is frozen completely and the ice is being sensibly sub-cooled. The refrigeration unit and the pump are switched off, and the frozen test capsule is kept inside the charging tank to maintain its temperature until finishing the preparation of the discharging experiment (which takes few minutes).

Prior to discharging experiments, the manual gate valves on the piping system are positioned for the discharging mode. The digital thermostat is set at one of the five test temperatures mentioned in Table 1. The pump is switched on and the refrigeration unit operates only during the preparation to cool the circulating HTF. Once the adjusted HTF temperature is reached, both of the refrigeration unit and the pump are switched off. The next step is to close the manual gate valves of the evaporator and open those of the heating section. The pump and the heating section are switched on. The heating section is controlled by the digital thermostat. The PCM temperature of the frozen spherical capsule is fixed at −8 °C as an initial PCM temperature for all discharging experiments. The volume flow rate of the HTF is set at one of the five volume flow rates mentioned in Table 1. The next step is to run the data acquisition software and transmit rapidly the spherical capsule from the charging tank to the discharging one. Measurements of the PCM temperatures inside the spherical

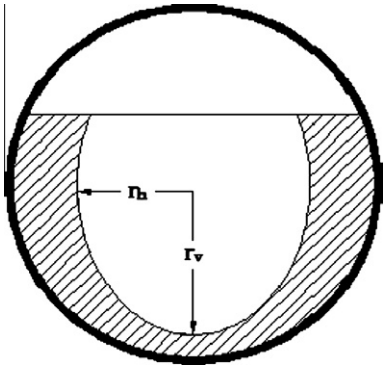

Figure 2a Sketch of the solidified volume of the PCM.

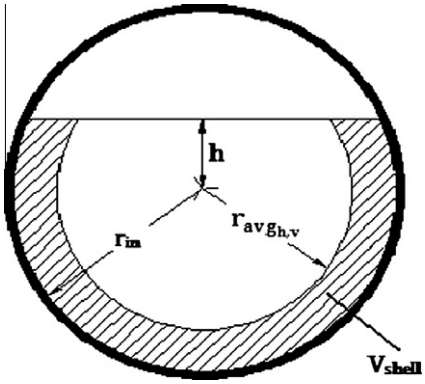

Figure 2b Sketch of the solidified volume of the PCM after simplification.

capsule and the HTF temperatures around it are scanned and recorded every 2 s by the data acquisition system. The experiment is terminated when the temperature of the PCM inside the spherical capsule begins to approach that of the HTF. This indicates that the ice is melted completely and the water is being sensibly super-heated. The electric heater and the pump are then switched off.

4. Data reduction

Through all the charging experiments, the test sphere is filled by 80% of its internal volume with PCM (distilled water) and care is taken to ensure that the test capsule is immersed in the middle of the charging tank. Also, the HTF flows upward around the test capsule. Consequently, a symmetric solidification around the vertical axis of the test capsule is assumed. Fig. 2a shows a sketch of the solidified volume of the PCM formed inside the test spherical capsule. This figure clarifies the symmetric solidification around the vertical axis of the test capsule, but it is clear that the development of ice is different in both the horizontal and vertical axes. So, one may simplify the solidified volume by taking the arithmetic average of the horizontal and vertical radii of the solid–liquid interface as shown in Fig. 2b. According to Fig. 2b, the spherical shell volume is calculated according to the following formula:

$$V_{shell} = (2/3)\pi(r^3_{avg_{h,v}}) + \pi h(r^2_{in} - r^2_{avg_{h,v}})$$

where V_{shell} is the spherical shell volume m^3, r_{in} is the internal radius of the test spherical capsule m, r_h is the horizontal radius of solid–liquid interface in test capsule m, r_v is the vertical radius of solid–liquid interface in test capsule m, $r_{avg_{h,v}}$ is the arithmetic average radius $(= \frac{r_h + r_V}{2})$ m, and h is the vertical distance, measured from the center of the spherical capsule to the free surface of the encapsulated PCM m.

4.1. Solidified mass m_s and melted mass m_m

The solidified mass of the PCM is calculated from:

$$m_s = \rho(\rho_w/\rho_i)V_{shell}$$

and the melted mass of the PCM is calculated from:

$$m_m = \rho_w V_{shell}$$

4.2. Accumulative stored andregained thermal energy Q_{st} & Q_{reg}

The accumulative thermal energy stored within the test capsule is derived as follows:

$$Q_{st} = \rho_w V_o \left\{ C_w(T_o - T_1) + \left(\frac{m_s}{m_o}\right)(L.H.) + \left(\frac{m_s}{m_o}\right) C_i(T_{pc} - T_s) \right\}$$

and the accumulative thermal energy regained from the melted PCM formed within the test spherical capsule is calculated from following equation:

$$Q_{reg} = \rho_w V_o \left\{ C_i(T_s - T_o) + \left(\frac{m_m}{m_o}\right)(L.H.) + \left(\frac{m_m}{m_o}\right) C_i(T_1 - T_{pc}) \right\}$$

4.3. Charging rate $\dot{Q}_{ch}$ and discharging rate $\dot{Q}_{dis}$

The charging rate of thermal energy stored within the test capsule is calculated from;

$$\dot{Q}_{ch} = \frac{\Delta Q_{st}}{\Delta t}$$

The discharging rate of thermal energy regained from the test capsule is calculated from;

$$\dot{Q}_{ch} = \frac{\Delta Q_{reg}}{\Delta t}$$

4.4. Energy recovery ratio (ERR)

$$\mathrm{ERR} = \frac{\mathrm{Q}_{reg}/\mathrm{t}_{\mathrm{comp,dis}}}{\mathrm{Q}_{st}/t_{\mathrm{comp,ch}}}$$

4.5. Dimensionless temperature (T^*) and dimensionless time (τ)

Dimensionless temperature (T^*) is defined as the ratio of the temperature of PCM at the center of spherical capsule to the phase change temperature of PCM. It is computed from the following equation:

$$T^* = \frac{T_c}{T_{pc}}$$

Dimensionless time (τ) is expressed as Fourier number (F_O). Conceptually, it is the ratio of the heat conduction rate to the rate of thermal energy storage. It is defined as:

$$\tau = F_O = \frac{\alpha_i \times t}{r_{in}^2}$$

4.6. Solidified mass fraction and melted mass fraction

Solidified mass fraction is defined as the ratio of the solidified mass to the mass of the PCM encapsulated inside the spherical capsule. Thus, the solidified mass fraction is calculated from the following formula:

$$\text{Solidified mass fraction} = \frac{m_s}{m_o} = \frac{\rho_i \cdot V_s}{\rho_w \cdot V_o}$$

Melted mass fraction is defined as the ratio of the melted mass to the mass of the PCM encapsulated inside the spherical capsule. Accordingly, the melted mass fraction is computed from the following formula:

$$\text{Melted mass fraction} = \frac{m_m}{m_o}$$

4.7. Percentage of energy stored and percentage of energy regained

The percentage of energy stored within a test capsule is defined as the ratio of accumulative energy stored at any charging time to the maximum energy stored at the complete charging time, namely;

$$\%\text{Energy stored} = \frac{Q_{st}}{Q_{st,max}} \times 100$$

The percentage of energy regained from a test capsule is defined as the ratio of accumulative energy regained at any discharging time to the maximum energy regained at the complete discharging time, namely;

$$\%\text{Energy regained} = \frac{Q_{reg}}{Q_{reg,max}} \times 100$$

5. Results and discussion

Through the present chapter, the experimental results concerning the effect of capsule material, capsule size, HTF temperature, and the volume flow rate of HTF on the dimensionless time for complete charging/discharging, the solidified/melted mass fraction, the percentage of energy stored/regained, and the charging/discharging rate are analyzed, compared and discussed.

5.1. Charging process results

5.1.1. Effect of capsule material

The effect of the material of the spherical capsule on the dimensionless time for complete charging is shown in Fig. 3. The tested materials are copper, brass, stainless steel, glass, and plastic. It is indicated that for the same operating conditions, the metallic capsules introduced lower dimensionless time for complete charging, especially the copper capsule which took the lowest dimensionless time. Also, it is interesting to notice that the difference between the times for complete charging when using either metallic or non metallic capsules is relatively small. This small difference makes the use of the non metallic capsules is more economical. For further exploring, Fig. 4 presents the effect of the capsule material on the variation of the solidified mass fraction with the dimensionless time, τ, during the charging process while keeping the rest of parameters unchanged. It is noticed that for all test materials, the solidified mass fraction increases as the dimensionless time increases. Also, for a given dimensionless time, the magnitude of the solidified mass fraction increases by increasing the thermal conductivity of the capsule material. For that aspect, the copper capsule introduces the highest solidified mass fraction, while the nonmetallic capsules produce the lowest one. It is also noticed that for all capsule materials the rate of increase of the mass fraction at the beginning is faster than that at the end of the solidification process. This can be attributed to the fact that the progressive formed ice layer acts as an insulating material for the rest of the contained water.

Fig. 5 indicates the effect of the capsule material on the variation of the percentage of energy stored with the dimensionless time during the charging process, while keeping the other parameters unchanged. It is realized that the percentage

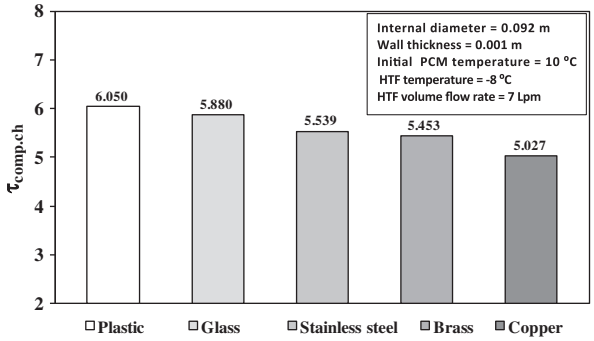

Figure 3 Effect of the capsule material on the dimensionless time for complete charging.

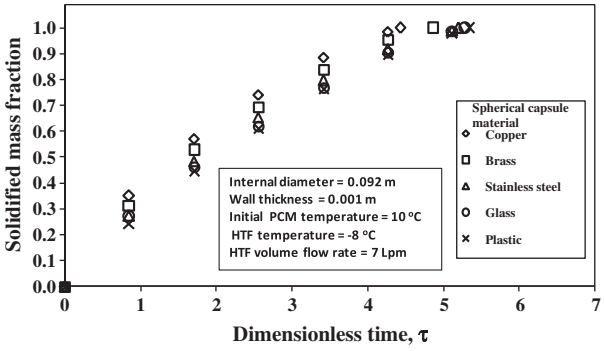

Figure 4 Variation of the solidified mass fraction with the dimensionless time using different capsule materials during the charging process.

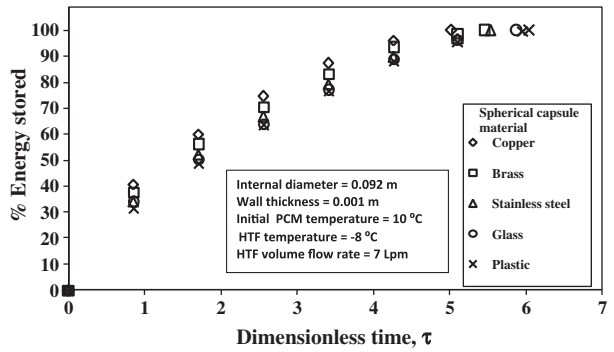

Figure 5 Variation of the percentage of energy stored with the dimensionless time using different capsule materials during the charging process.

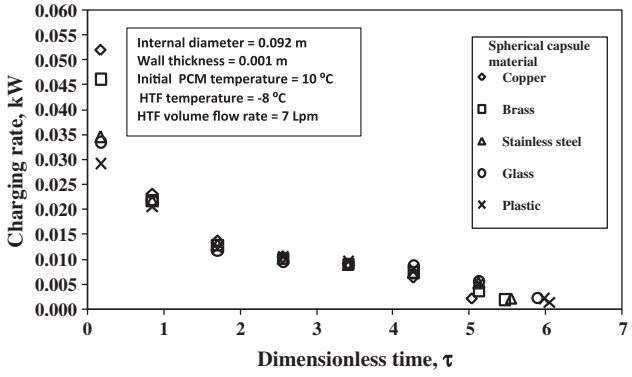

Figure 6 Variation of the charging rate with the dimensionless time using different capsule materials during the charging process.

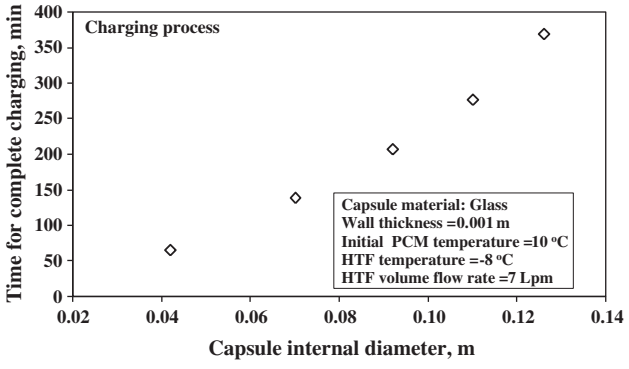

Figure 7 Effect of the capsule size on the time for complete charging.

of energy increases as dimensionless time increases. It is also noticed that for a given dimensionless time, copper and brass capsules store more energy rather than stainless steel and non metallic capsules. This is due to their better thermal conductivity and accordingly they took relatively short dimensionless times for complete charging. Moreover, Fig. 6 shows the variation of the charging rate (energy stored rate) with the dimensionless time during the charging process. The results of the different test capsule materials are presented for comparison. It is shown that at the beginning of the charging

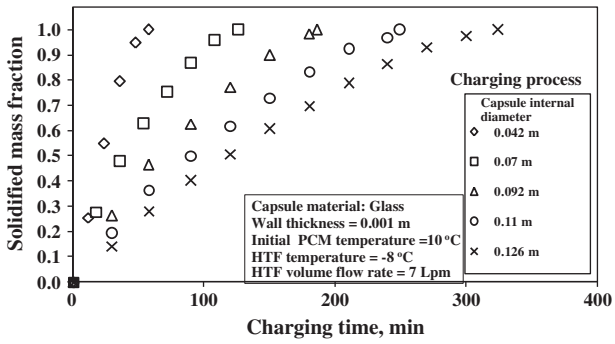

Figure 8 Variation of the solidified mass fraction with the charging time using different capsule sizes.

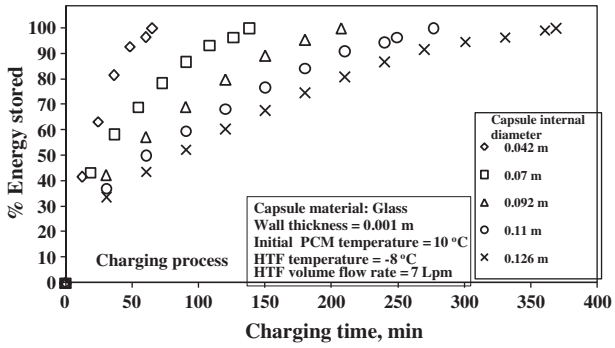

Figure 9 Variation of the percentage of energy stored with the charging time using different capsule sizes.

process, the charging rate of the metallic capsules is higher than that of the nonmetallic ones. After that, the charging rate of all capsules is rapidly decreased and their values are coincident. This behavior is related to the decrease in the temperature difference between the PCM and HTF.

5.1.2. Effect of capsule size

In the present study, the glass capsule is chosen to investigate the effect of capsule size on the characteristics of the charging and the discharging processes. Fig. 7 shows the variation of the capsule internal diameter with the charging time. The results ensure the increase of the charging time with increasing the capsule size. Moreover, Fig. 8 shows the variation of the solidified mass fraction with the charging time. The results are presented for comparison. It is noticed that; the solidified mass fraction increases with increasing of the charging time for all capsule sizes. Also, it is realized that for a given charging time, the solidified mass fraction of smaller capsule size is greater than that of bigger one.

Furthermore, Fig. 9 clarifies the variation of the percentage of energy stored within a capsule with the charging time. The data of all capsule sizes are compared. Similar trend is observed for all capsule sizes. It is noticed that for a given capsule size, increasing the charging time; increases the percentage of energy stored. Also, for a given charging time, increasing the capsule size; increases the percentage of energy stored. On the other hand, one can observe from Fig. 10 that as the charging time is increased, the curves of charging rate of all capsule sizes seem

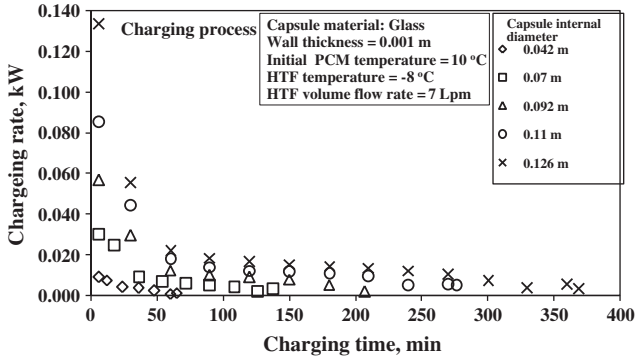

Figure 10 Variation of the charging rate with the charging time using different capsule sizes.

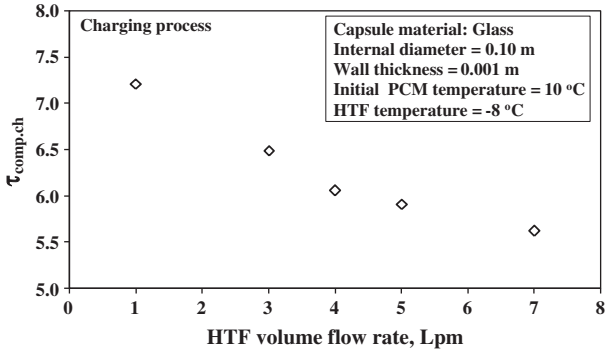

Figure 11 Effect of the HTF volume flow rate on the dimensionless time for complete charging.

to be closer together. Also, it is indicated that the higher charging rate is associated with the larger capsule size. For all capsule sizes, increasing the charging time; decreases the charging rate. This behavior is attributed to the fact that as the charging time increases, the temperature difference between the PCM and HTF is decreased.

5.1.3. Effect of HTF volume flow rate

The glass capsule is selected to investigate the effect of HTF volume flow rate on the characteristics of the charging and the discharging processes. Fig. 11 shows the variation of the dimensionless time for complete charging with the HTF volume flow rate. It is observed that increasing the HTF volume flow rate; decreases the dimensionless time for complete charging. The effect of the HTF volume flow rate on the variation of the solidified mass fraction with the dimensionless time during the charging process is shown in Fig. 12. It is indicated that for all HTF volume flow rates, increasing the dimensionless time increases the solidified mass fraction till reaching the time for complete solidification (the solidified mass fraction equals to unity). Also, it is observed that for a given dimensionless time, the solidified mass fraction increases by increasing the HTF volume flow rate. Accordingly, the higher the HTF volume flow rate, the shorter the dimensionless time for complete charging.

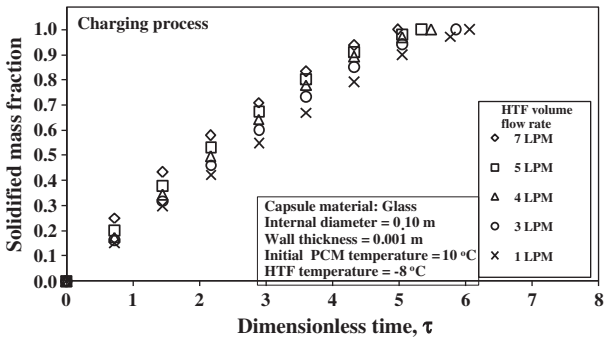

Figure 12 Variation of the solidified mass fraction with the dimensionless time using different HTF volume flow rates during the charging process.

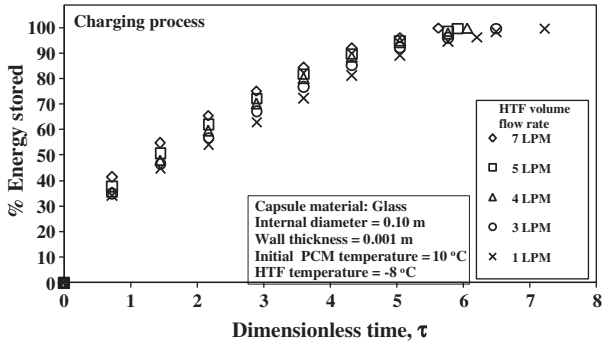

Figure 13 Variation of the percentage of energy stored with the dimensionless time using different HTF volume flow rates during the charging process.

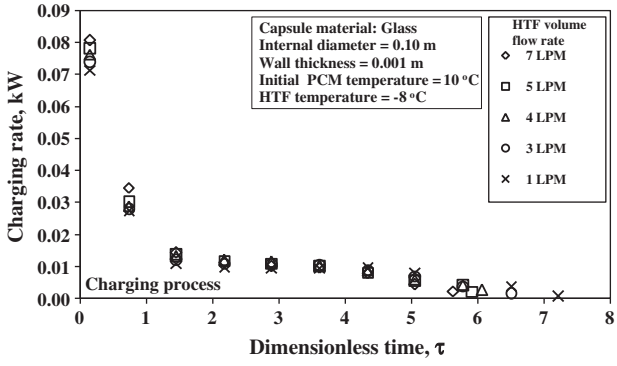

Figure 14 Variation of the charging rate with the dimensionless time using different HTF volume flow rates during the charging process.

To further explore, Fig. 13 depicts the effect of the HTF volume flow rate on the relation between the percentage of energy stored and the dimensionless time during the charging process. Different volume flow rates introduce similar trend. It is shown that for a given HTF volume flow rate, increasing the dimensionless time; increases the percentage of energy stored. Also, for a given dimensionless time, higher HTF volume flow rate introduces higher percentage of energy stored. It

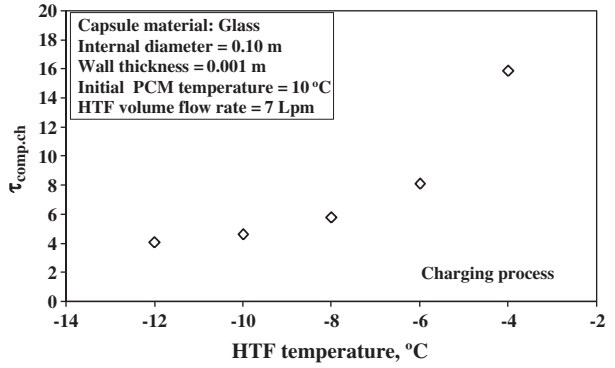

Figure 15 Effect of the HTF temperature on the dimensionless time for complete charging.

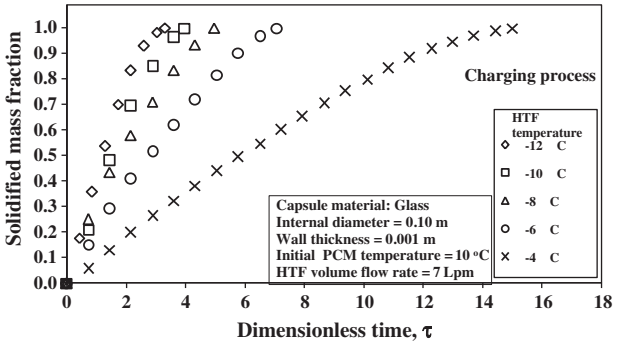

Figure 16 Variation of the solidified mass fraction with the dimensionless time using different HTF temperatures during the charging process.

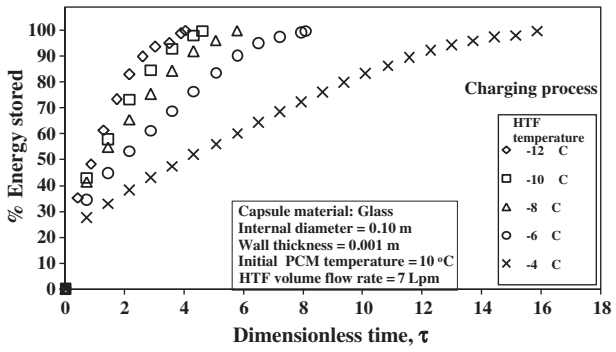

Figure 17 Variation of the percentage of energy stored with the dimensionless time using different HTF temperatures during the charging process.

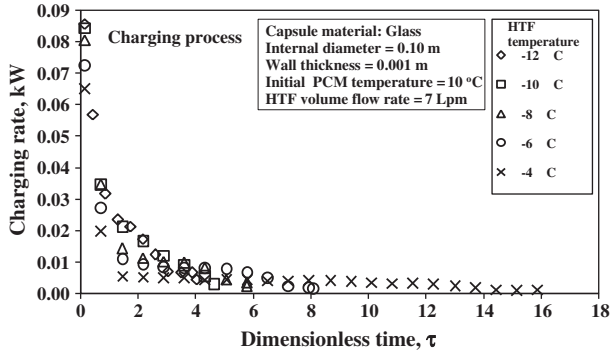

Figure 18 Variation of the charging rate with the dimensionless time using different HTF temperatures during the charging process.

can be observed from Fig. 14 that for a given HTF volume flow rate, as the dimensionless time increases, the charging rate of energy stored decreases. Also, the curves of charging rate with dimensionless time are coincident. Also, it is observed that at the beginning of charging process, higher charging rate is associated with higher HTF volume flow rate.

5.1.4. Effect of HTF temperature

Through the present study, the glass capsule is selected to investigate the effect of HTF temperature on the characteristics of the charging and the discharging processes. The temperature of HTF is varied from −4 °C to −12 °C. The HTF volume flow rate is kept at 7 Lpm, the internal capsule diameter is kept at 0.1 m and the initial PCM temperature is maintained at 10 °C. Fig. 15 depicts the variation of the HTF temperature with the dimensionless time for complete charging. It can be seen that the decrease of the HTF temperature from −4 °C to −12 °C reduces greatly the dimensionless time for complete charging. Furthermore, the results presented in Fig. 16 ensure those of Fig. 15 in the sense that lowering the HTF temperature; decreases the dimensionless time for complete solidification (the time for solidified mass fraction to be equal to unity).

One can observe from Fig. 17 that as the HTF temperature decreases, the percentage of energy stored increases. Consequently, the lower the HTF temperature, the shorter the dimensionless time for complete charging. This agrees with the previous results. Moreover, Fig. 18 shows the effect of the HTF temperature on the variation of the charging rate (rate of energy stored) with the dimensionless time. It is seen that the charging rate is rapidly decreased by increasing the dimensionless time. The data for all HTF temperatures have the same trend and are closer together.

5.2. Discharging process results

5.2.1. Effect of capsule material

Fig. 19 presents the effect of the capsule material on the dimensionless time for complete discharging. The rest of parameters are kept unchanged. It is shown that the metallic capsules introduce lower dimensionless time for complete discharging. On the other hand, Fig. 20 shows the variation of the melted mass fraction with the dimensionless time during a discharging process. The data of different test capsule materials are presented for comparison. It is seen that as the dimensionless time increases, the melted mass fraction increases. One can observe that the increase in the melted mass fraction for metallic capsules is higher than that of nonmetallic ones. For that aspect, the dimensionless time for complete discharging for metallic capsules is shorter than that of nonmetallic ones. Also, it is ob-

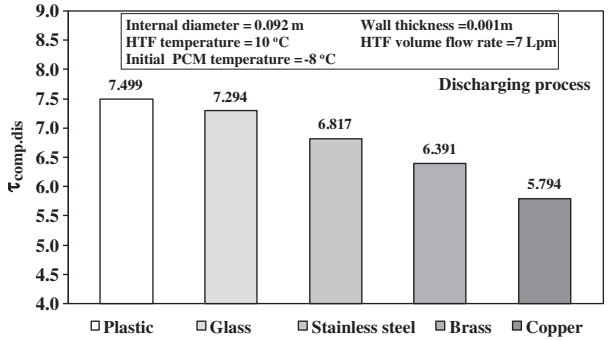

Figure 19 Effect of the capsule material on the dimensionless time for complete discharging.

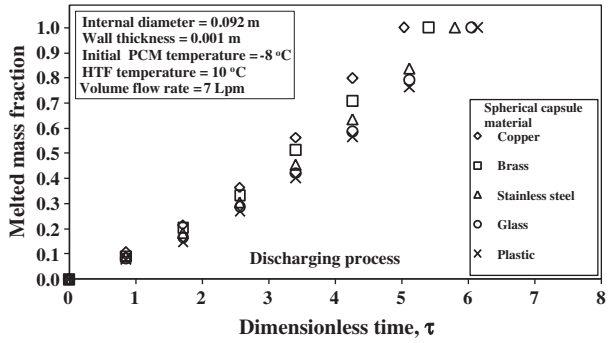

Figure 20 Variation of the melted mass fraction with the dimensionless time using different capsule materials during the discharging process.

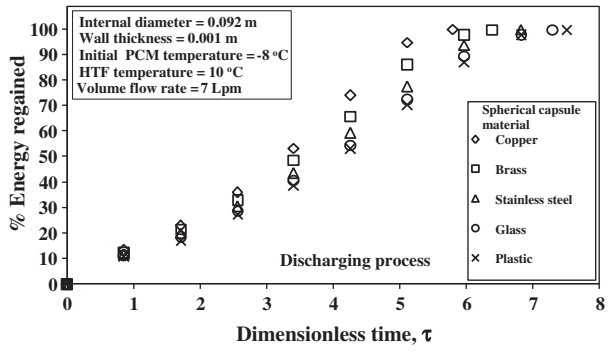

Figure 21 Variation of the percentage of energy regained with the dimensionless time using different capsule materials during the discharging process.

served that the whole capsule materials have the same trend in the sense that at the beginning of the discharging process, the melted mass fraction increases slowly with time compared to that at the end of the melting process. This can be attributed to the fact that at the beginning, the formed melted layer between the inner surface of the capsule and the remaining ice is small. Accordingly, the heat transfer by conduction is the dominant, while the convective heat transfer is not effective. As time goes, the gap of melting layer increases and consequently, the heat transfer by convection is enhanced, that lead to increase the melting rate.

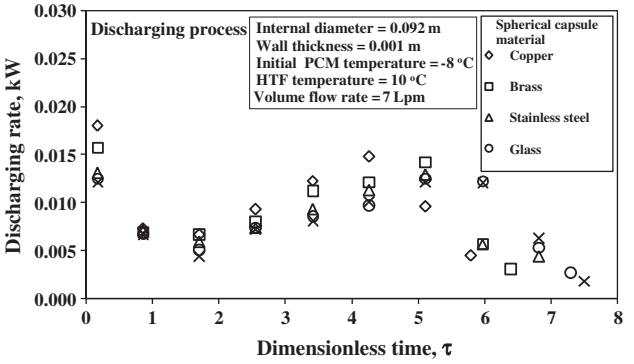

Figure 22 Variation of the discharging rate with the dimensionless time using different capsule materials during the discharging process.

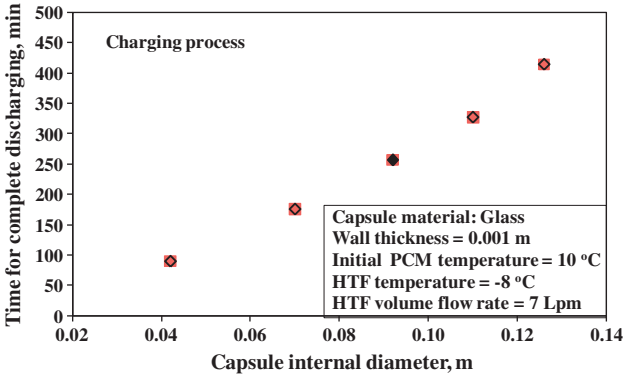

Figure 23 Effect of the capsule size on the time for complete discharging.

To further explore, Fig. 21 depicts the variation of the percentage of energy regained with the dimensionless time during the discharging process. The results of the different test capsule materials are presented for comparison. One can observe that the increasing of the dimensionless time increases the percentage of energy regained. This is true for all capsule materials. Also, it is realized that the nonmetallic capsules consumes its stored energy in a relatively longer time rather than the metallic ones. Fig. 22 presents the variation of the discharging rate with the dimensionless time during the discharging process. The data of all test capsule materials are compared. The results of the capsule materials have the same trend. It is noticed that at the beginning of discharging process, high discharging rate is happened, which can be attributed to the high temperature difference between the HTF and PCM. After that, the discharging rate decreases suddenly due to the fast decrease in temperature difference during the sensible heating of ice till reaching the phase change temperature. As mentioned earlier, increasing the melting layer by passing the time enhances the heat transfer by convection. So, the discharging rate increases gradually till finishing the melting process. Finally; the discharge rate decreases as a result of the decrease in the temperature difference between the HTF and PCM. Also, it is observed that the discharging rate of nonmetallic capsules takes longer time than those of metallic ones.

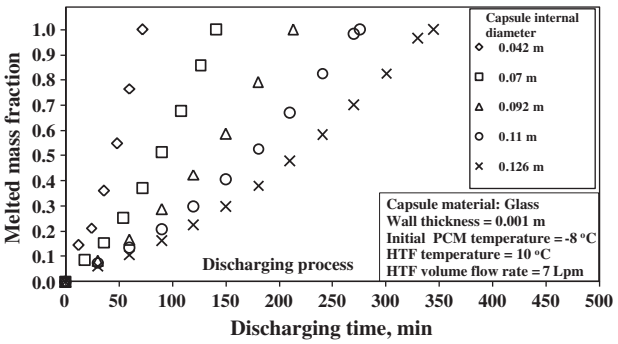

Figure 24 Variation of the melted mass fraction with the discharging time using different capsule sizes.

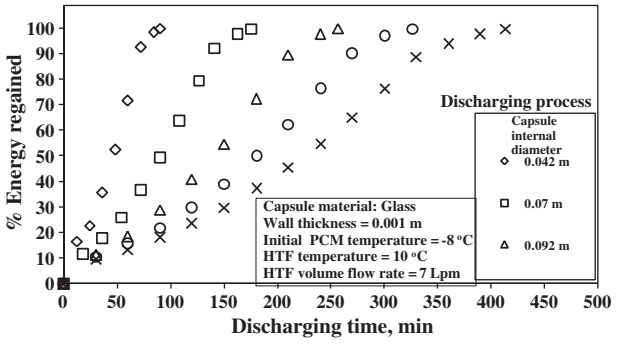

Figure 25 Variation of the percentage of energy regained with the discharging time using different capsule sizes.

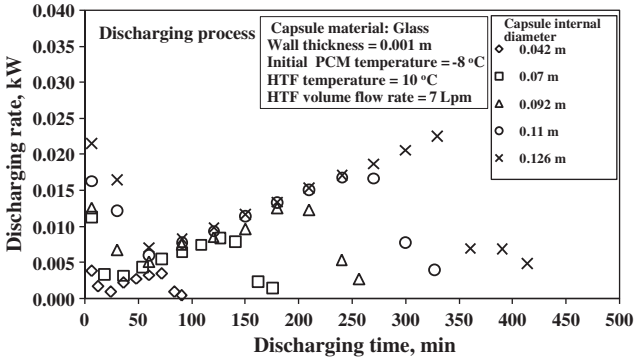

Figure 26 Variation of the discharging rate with the discharging time using different capsule sizes.

5.2.2. Effect of capsule size

It is indicated from Fig. 23 that increasing the capsule size increases the time for complete discharging. Moreover, Fig. 24 indicates the effect of the capsule size on the variation of the melted mass fraction with the discharging time. This figure reveals that for a given discharging time, the melted mass fraction is decreased by increasing the capsule size. Also, it is noticed that for a given capsule size, the melted mass fraction is increased by increasing the discharging time.

The effect of the capsule size on the relation between the percentage of energy regained and the discharging time is shown in Fig. 25. It is noticed that for a given capsule size, the melted mass fraction is increased by increasing the discharging time. Also, it is observed that for a given discharging time, the larger the capsule size, the lower the percentage energy regained. Accordingly, the larger the capsule size, the longer the time for complete discharging. Fig. 26 reveals the relation between the discharge rate and the discharging time. The data for all capsule sizes are presented for comparison. It is observed that the data for all capsule sizes have the same trend in the sense as discussed earlier (Section 5.2.1). Also, it is shown that the largest capsule size introduces the longest discharging time.

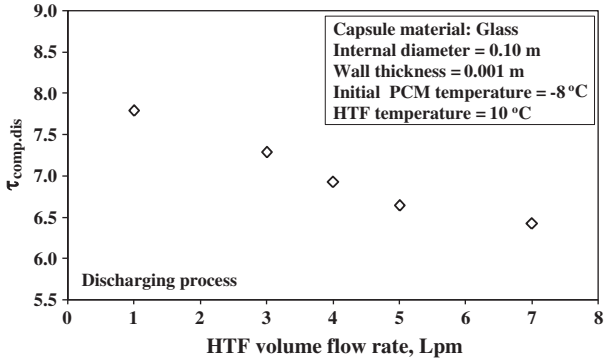

Figure 27 Effect of the HTF volume flow rate on the dimensionless time for complete discharging.

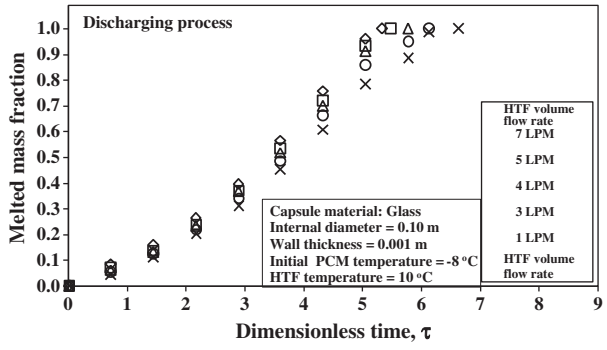

Figure 28 Variation of the melted mass fraction with the dimensionless time using different HTF volume flow rates during the discharging process.

5.2.3. Effect of HTF volume flow rate

It is realized from Fig. 27 that increasing the HTF volume flow rate, decreases the time for complete discharging. Furthermore, Fig. 28 reveals the variation of the melted mass fraction with the dimensionless time during the discharging process. The data of all tested HTF volume flow rates are compared. All the data introduced the same trend. It is shown that increasing the dimensionless time, increases the melted mass fraction. It is also observed that for a given dimensionless time, the melted mass fraction is increased by increasing the HTF volume flow rate.

The effect of the HTF volume flow rate on the relation between the percentage of energy regained and the dimensionless time during the discharging process is shown in Fig. 29. It is

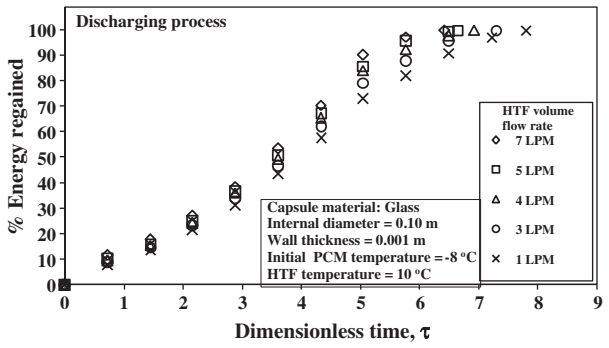

Figure 29 Variation of the percentage of energy regained with the dimensionless time using different HTF volume flow rates during a discharging process.

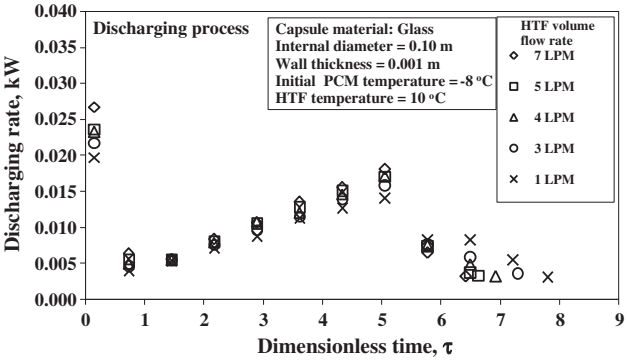

Figure 30 Variation of the discharging rate with the dimensionless time using different HTF volume flow rates during the discharging process.

revealed that for a given dimensionless time, increasing the HTF volume flow rate increases the percentage of energy regained. Also, for a given HTF volume flow rate, the percentage of energy regained is increased by increasing the dimensionless time. Fig. 30 reveals the variation of the discharging rate with the dimensionless time during the discharging process. The results of the HTF volume flow rates are compared. These results ensure that the discharging rate is decreased by increasing the dimensionless time. Also, it is noticed that the results of all the HTF volume flow rates have the same trend. The reason for this behavior is discussed in Section 5.2.1.

5.2.4. Effect of HTF temperature

Fig. 31 presents the effect of the HTF temperature on the dimensionless time for complete discharging. It is indicated that decreasing the temperature of the HTF, increases the dimensionless time for complete discharging. On the other side, Fig. 32 depicts the relation between the melted mass fraction and the dimensionless time during the discharging process. The data for all tested HTF temperatures are compared. It is shown that for a given HTF temperature, the melted mass fraction is increased by increasing the dimensionless time. The results of all test HTF temperatures have the same trend. Also, it is observed that for a given dimensionless time, the melted mass fraction is increased by increasing the HTF temperature.

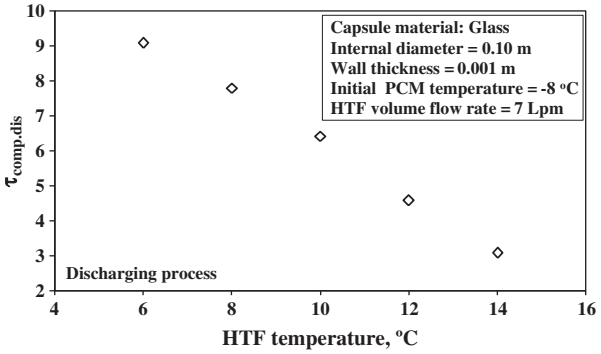

Figure 31 Effect of the HTF temperature on the dimensionless time for complete discharging.

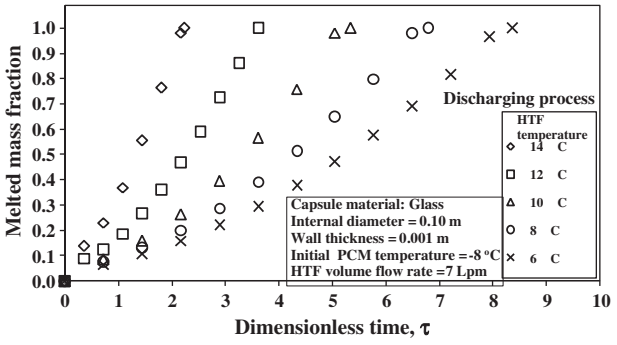

Figure 32 Variation of the melted mass fraction with the dimensionless time using different HTF temperatures during the discharging process.

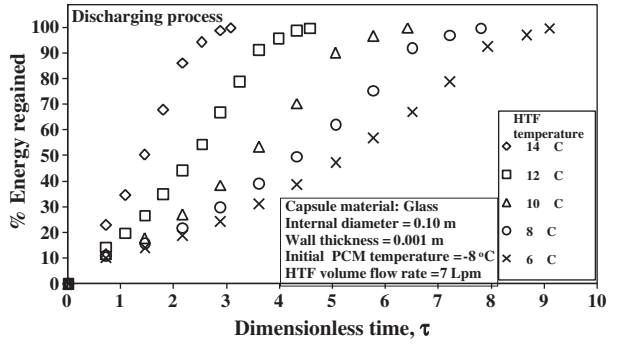

Figure 33 Variation of the percentage of energy regained with the dimensionless time using different HTF temperatures during the discharging process.

Moreover, Fig. 33 reveals that the percentage of energy regained is increased by increasing the HTF temperature for a given dimensionless time. Also, for a given HTF temperature, the percentage of energy regained is increased by increasing the discharging time. One can observe from Fig. 34 that the discharging rate using a given HTF temperature is decreased by increasing the dimensionless time. In addition, for a given dimensionless time, the discharging rate is higher for high HTF temperatures. The reason for this behavior is related to the progressive convection effect by passing the time as mentioned earlier.

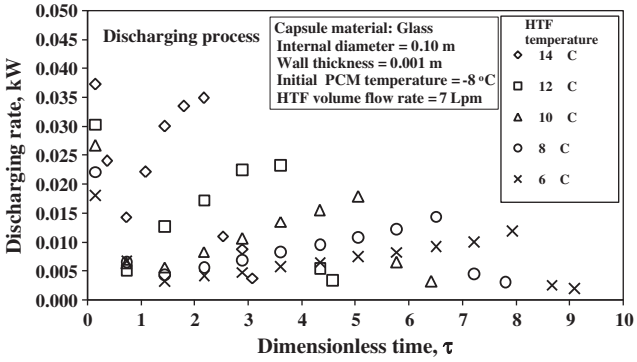

Figure 34 Variation of the discharging rate with the dimensionless time using different HTF temperatures during the discharging process.

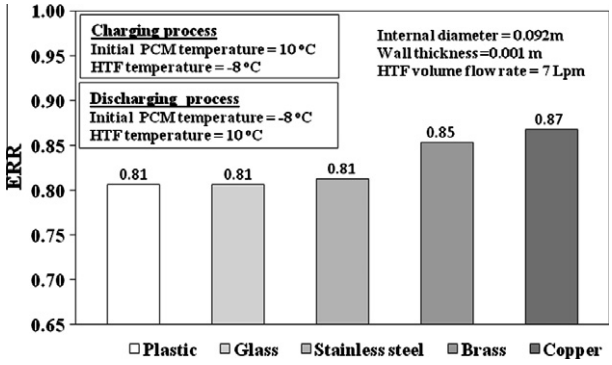

Figure 35 Effect of the capsule material on ERR.

5.3. Energy recovery ratio

The energy recovery ratio (ERR) is defined as the ratio of the average energy regained rate to the average energy stored rate under the same operational conditions. The energy storage performance is measured by the energy recovery ratio, the higher the energy recovery ratio, the better the energy storage performance. Fig. 35 reveals the effect of capsule material on the ERR while the rest of parameters are unchanged. The data for all test capsule materials are compared. It is noticed that the copper capsule introduce the highest ERR. Also, the plastic capsule introduce an acceptable ERR compared to those of higher thermal conductivities. Accordingly, the use of nonmetallic capsules is encouraging for its economical aspects (cheap and easy to fabricate). On other side, Fig. 36 shows the effect of the capsule size (capsule internal diameter) on the parameter ERR. It is indicated that the higher the capsule size, the higher ERR. Furthermore, Fig. 37 depicts the effect of HTF volume flow rate on the parameter ERR. It is observed that the lowest HTF volume flow rate introduces the highest value of ERR.

6. Comparisons with the available published data

Fig. 38 shows a comparison between the present results and the numerical results of Ismail et al. [3] for the variation of solidified mass fraction with the charging time. The comparison ensures reasonable agreement between the present results and those of [3]. The slight discrepancy between them is related to the difference between the present operating conditions and those of [3].

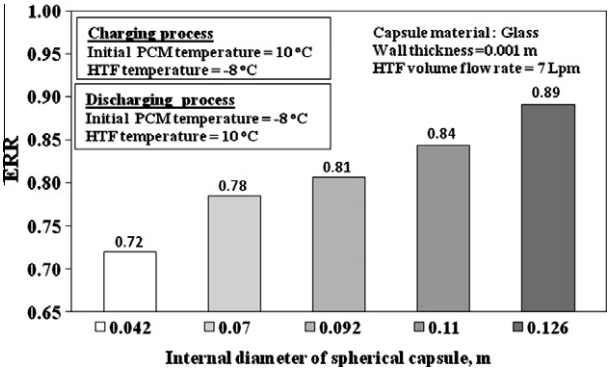

Figure 36 Effect of the capsule size on ERR.

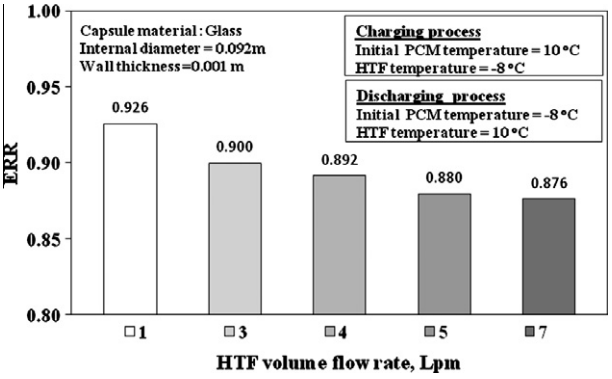

Figure 37 Effect of the HTF volume flow rate on ERR.

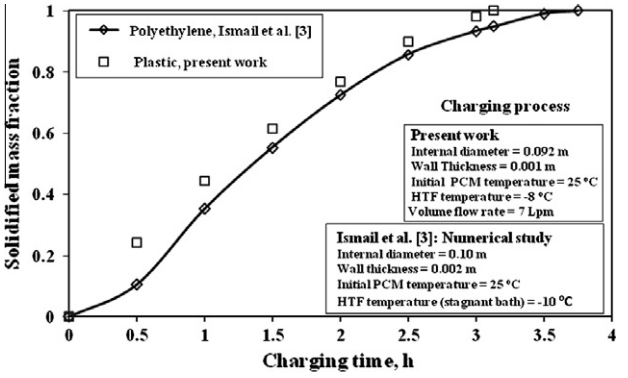

Figure 38 Comparison between the present experimental study and the results of Ismail et al. [3].

7. Conclusions

Based on the present results, the following significant features can be drawn:

1. The time for complete charging is decreased by using metallic capsules, smaller capsule sizes, lower HTF temperatures and higher HTF volume flow rates.
2. The solidified mass fraction is increased by employing metallic capsules, using smaller capsule sizes, higher HTF volume flow rates and lower HTF temperatures.

3. The percentage of the energy stored is increased by using metallic capsules, bigger capsule sizes, higher HTF volume rates and lower HTF temperatures.
4. The time for complete discharging is increased by using nonmetallic capsules, bigger capsule sizes, lower HTF temperatures and lower volume flow rates.
5. The melted mass fraction and the percentage of the energy regained are increased by employing metallic capsules, using smaller capsule sizes, higher HTF volume flow rates and higher HTF temperatures.
6. The energy recovery ratio is becoming better, when using metallic capsules, increasing the capsule size and reducing the HTF volume flow rates.
7. The thermal conductivity of the capsule material has a relatively small effect on the time for complete charging, time for complete discharging, solidified mass fraction, melted mass fraction and the energy recovery ratio.
8. Although shorter time is consumed for the charging process using the metallic capsules, significant longer time is taken for the discharging process when using the nonmetallic capsules, which lead to select the later type to enhance the thermal energy storage system.
9. It is economical to use nonmetallic capsules (cheap and easy to fabricate), as the change in time for complete charging and discharging as well as ERR is small.
10. The gained results of the present research are confident as reasonable agreement is noticed when compared with the results of one of the literature.

References

[1] Eames W, Adref KT. Freezing and melting of water in spherical enclosures of the type used in thermal (Ice) storage systems. Appl Therm Eng 2002;22:733–45.

[2] Jung In Yoon, Choon Geun Moon, Eunpil Kim, Young Seok Son, Jae Dol Kim, Toyofumi Kato. Experimental study on freezing of water with supercooled region in a horizontal cylinder. Appl Therm Eng 2001;21:657–68.

[3] Ismail KAR, Henriquez JR, da Silva TM. A parametric study on ice formation inside a spherical capsule. Int J Therm Sci 2003;42:881–7.

[4] Sakr MH, Abdel-Aziz RM, Ghorab AAE. Experimental and theoretical study on freezing and melting in capsules for thermal storage. ERJ Soubra Faculty Eng 2008;9:48–65.

[5] Tan FL, Hosseinizadeh SF, Khodadadi JM, Fan Liwu. Experimental and computational study of constrained melting of phase change materials (PCM) inside a spherical capsule. Int J Heat Mass Trans 2009;52:3464–72.

[6] Cheralathan M, Velraj R, Renganarayanan S. Heat transfer and parametric study of an encapsulated phase change material based cool thermal energy storage system. J Zhejiang Univ Sci A 2006;7(11):1886–95.

[7] Kousksou T, Bedecarrats JP, Dumas JP, Mimet A. Dynamic modelling of the storage of an encapsulated ice tank. Appl Therm Eng 2005;25:1534–48.

[8] Ismail KAR, Henriquez JR. Solidification of PCM inside a spherical capsule. Energy Convers Manage 2000;41:173–87.

[9] Kalaiselvam S, Veerappan M, Arul Aaron A, Iniyan S. Experimental and analytical investigation of solidification and melting characteristics of PCMs inside cylindrical encapsulation. Int J Therm Sci 2008;47:858–74.

[10] Khodadadi JM, Zhang Y. Effects of buoyancy-driven convection on melting within spherical containers. Int J Heat Mass Trans 2001;44:1605–18.

[11] Wu T, Liaw HC, Chen YZ. Thermal effect of surface tension on the inward solidification of spheres. Int J Heat Mass Trans 2002;45:2055–65.

[12] MacPhee David, Dincer Ibrahim. Thermal modeling of a packed bed thermal energy storage system during charging. Appl Therm Eng 2009;29:695–705.

[13] Erek Aytunc, Dincer Ibrahim. Numerical heat transfer analysis of encapsulated ice thermal energy storage system with variable heat transfer coefficient in downstream. Int J Heat Mass Trans 2009;52:851–9.

[14] MacPhee David, Dincer Ibrahim. Performance assessment of some ice TES systems. Int J Therm Sci 2009;xxx:12.

[15] Ananthanarayanan V, Sahai Y, Mobley CE, Rapp RA. Modeling of fixed bed heat storage units utilizing phase-change materials. Metall Trans B 1987;18:339–46.

[16] Beasley DE, Ramanarayanan C. Thermal response of a packed bed of spheres containing a phase change material. Int J Energy Res 1989;13:253–65.

[17] Sozen M, Vafai K, Kennedy LA. Thermal charging and discharging of sensible and latent heat storage packed beds. AIAA J Thermophys 1991;5(4):623–5.

[18] Ismail KAR, Stuginsky R. A parametric study on possible fixed bed models for PCM and sensible heat storage. Appl Therm Eng 1999;19(7):757–88.

[19] Properties of Working Fluids–Brines. M. CONDE Engineering, Zurich; 2002.

Dr. Reda I. Elghnam is currently Associate Professor of Mechanical Engineering (Power department) at Shoubra Faculty of engineering, Benha University, Egypt. He has published about 19 papers in referred national and international journals and conference proceedings. His area of research is heat transfer, heat pipes and combustion.

Dr. Ramdan A. Abdelaziz is currently Professor of Mechanical Engineering (Power department) at Shoubra Faculty of engineering, Benha University, Egypt. His area of research is heat transfer, heat pipes and refrigeration and air conditioning.

Dr. Mohamed H. Sakr is currently Professor of Mechanical Engineering (Power department) at Shoubra Faculty of engineering, Benha University, Egypt. His area of research is heat transfer, heat pipes and refrigeration and air conditioning.

Eng. Hany E. Abdelrhman is currently Associate Lecturer of Mechanical Engineering (Power department) at Shoubra Faculty of engineering, Benha University, Egypt. His area of research is heat transfer, heat pipes and refrigeration and air conditioning.